UCLA
UCLA Previously Published Works

Title
Infinite lifetime of underwater superhydrophobic states

Permalink
https://escholarship.org/uc/item/8hm781p6

Journal
Physical Review Letters, 113(3)

ISSN
0031-9007

Authors
Xu, M
Sun, G
Kim, CJ

Publication Date
2014-09-25

DOI
10.1103/PhysRevLett.113.136103

Supplemental Material
https://escholarship.org/uc/item/8hm781p6#supplemental

Peer reviewed

Infinite Lifetime of Underwater Superhydrophobic State

Muchen Xu, Guangyi Sun, and Chang-Jin "CJ" Kim[*]

Mechanical and Aerospace Engineering Department

University of California at Los Angeles (UCLA), Los Angeles, CA 90095, USA

Abstract

Submerged superhydrophobic (SHPo) surfaces are well known to transition from the dewetted to wetted state over time. Here, a theoretical model is applied to describe the depletion of trapped air in a simple trench and re-arranged to prescribe the conditions for infinite lifetime. By fabricating a microscale trench in a transparent hydrophobic material, we directly observe the air depletion process and verify the model. The study leads to the demonstration of infinite lifetime (> 50 days) of air pockets on engineered microstructured surfaces under water for the first time. Environmental fluctuations are identified as the main factor behind the lack of a long-term underwater SHPo state to date.

The stability of the air layer on superhydrophobic (SHPo [1]) surfaces fully submerged in water is of critical importance because their key anticipated applications, such as drag reduction [2-5] and anti-biofouling [6], are under water. Unfortunately, the air film on the underwater SHPo surface, often called a plastron, is fragile [2,7]. Over time, the air initially trapped on the SHPo surface diffuses away into the surrounding water, collapsing the air-water interface and causing a transition from the dewetted to wetted state [8]. Recent experimental studies showed that the lifetime of the underwater SHPo state is influenced by various environmental parameters [7,9-11]. However, most of the studies only reported statistical information, such as average wetting time; more direct knowledge such as air-depletion dynamics or the effect of roughness geometries is needed to design the SHPo surface to be more robust against wetting. While some underwater insects boast a long-term or even indefinite (tested up to 120 days [12]) plastron, all artificial SHPo surfaces retained their plastron for much shorter length of time (mostly less than

an hour; rarely for days [7,9,13-15]). To date, no artificial SHPo surface has been demonstrated to retain an air layer indefinitely unless assisted [16].

This paper aims to understand the air depletion process on submerged SHPo surfaces and to determine if an indefinite plastron is achievable. In order to systematically study the effect of geometric parameters of the surface structures for an intended goal, SHPo surfaces made of regular structures would be far more informative than those of random structures that produce only statistical data. Furthermore, for drag-reduction application in particular, SHPo surfaces with parallel trenches [3,4,17,18] have been found to outperform those with random structures [19,20], making SHPo surfaces with trenches a good candidate to study. Since multiple trenches are in parallel and isolated from each other, a single trench can represent the whole SHPo surface as far as the stability of the trapped air is concerned. The potential over-estimation of the depletion speed on single trench compared with the parallel trenches due to the edge effect [21,22] is considered minor to our goal. Importantly for our purpose instead, a sample with single trench would allow clear images of one air-water meniscus; in comparison, multiple menisci in multiple trenches would overlap and blur the images. The transparent sample with a single trench was fabricated by hot embossing Teflon® FEP into a deep-reactive-ion-etch (DRIE)-processed silicon mold by improving the process from [23], as described in Supplemental Material (SM). The whole Teflon® FEP sample is semi-clear and intrinsically hydrophobic with advancing contact angle ~115° [24]. Figure 1(a) shows scanning electron microscopy (SEM) images of the single-trench sample. The sidewall of the trench has nanometer-scale roughness, as it was replicated from the "scalloped" surface [25] on the DRIE silicon mold.
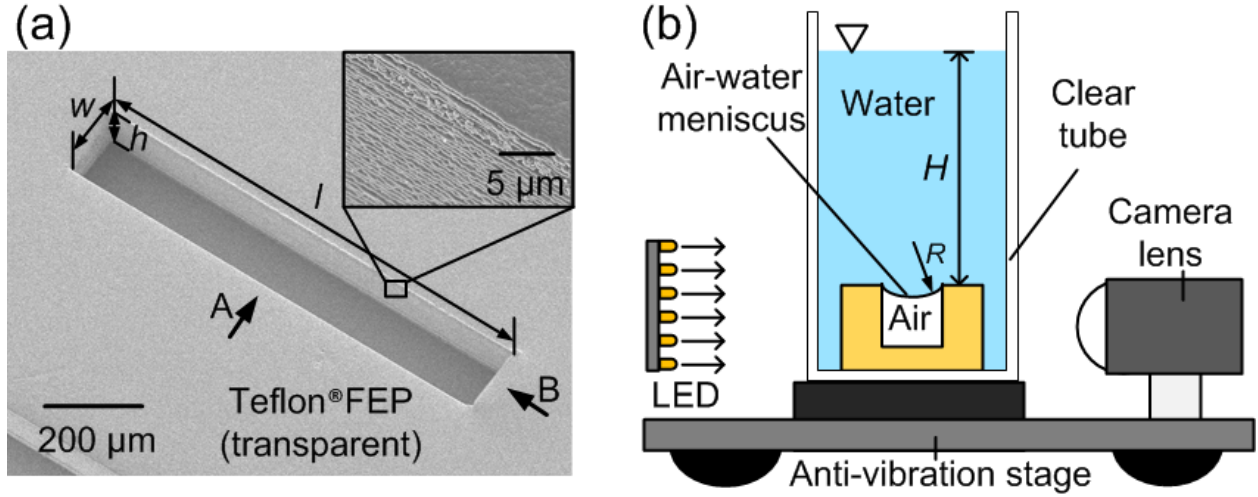
FIG. 1. The sample and testing setup. (a) SEM images of a single-trench sample with the microscale trench characterized by length l, width w, and depth h. (b) Schematic illustration of the experimental setup to visualize the air-water meniscus inside the trench throughout the depletion process. One sample was immersed in water of height H in a clear tube and observed from the side, as indicated by the arrow A in (a).

Let us first analyze how the trapped air is depleted from a hydrophobic trench after being submerged based on previous works [15,26,27]. Consider a simple trench with width w, length l, and depth h, as defined in Fig. 1(a), and the radius of curvature of the air-water interface R, as defined in Fig. 1(b). Since the trench length is much larger (~10 times) than its width, the meniscus was straight along the length of the trench in the middle section over a significant period of time before reaching the bottom, as shown in Fig. 2(a), supporting the 2D diffusion model as a crude but useful approximation. According to Henry`s law, the partial pressure of a gas equilibrated in water is: $p = k_H c$, where $k_H$ is Henry`s constant and c is the dissolved gas concentration in water. Right after submerging the sample from atmosphere (p_{atm}) to immersion depth H at hydrostatic pressure p_H, the air in the trench is compressed to $p_{tr,0}$ and the meniscus forms the radius of curvature R_0, as detailed in SM. If $p_{tr,0} > k_H c$, air in the trench will start to diffuse out through the meniscus. The volume rate of dissolution (i.e., the dissolution rate) of the trapped air into the water is limited by the diffusion of dissolved air in the water, which is related to the temporal and spatial evolvement of concentration field by Fick`s law approximated [27] as:

$$\frac{dV(t)}{dt} = -k_p A(t)[p_{tr}(t) - k_H c] \qquad (1)$$

where V is the air volume, k_p is the mass transfer coefficient of air across the air-water interface, p_{tr} is the air pressure in the trench, and A is the meniscus area or Eq. (S4). The influence of meniscus curvature on k_p was discussed in SM based on diffusion-limited drop evaporation theory [28]. To estimate the value of k_p, diffusion length was eventually applied for simplicity [15] as explained in SM. Combining Eq. (1) with the Laplace equation across the meniscus $p_{atm} + p_H - p_{tr} = \sigma / R$, where σ is the air-water interfacial tension, we get:

$$\frac{dV(t)}{dt} = -k_p A(t) [p_H - \frac{\sigma}{R(t)} + p_{atm} - k_H c] \tag{2}$$

Here, we consider only depinning impalement (not sagging [29,30]) because the trench is much deeper than it is wide. The wetting process goes through two stages: (i) Stage I involves the contact line pinned to the top edge of the trench, and (ii) Stage II involves the contact line sliding on the sidewall of the trench. For the pinned stage of Stage I, R can be numerically calculated with initial condition R_0 and boundary condition R_c, as detailed in SM. Since the depinning occurs when the angle of the meniscus on the sidewall reaches the advancing contact angle θ_{adv} [29], $R_c = w / 2\cos\theta_{adv}$. For the sliding stage of Stage II, since $R = R_c = \text{constant}$ for the simple trench, the meniscus slides down the vertical sidewall at constant speed $u = d(V / A) / dt$, which can also be obtained from Eq. (2). The meniscus movement was estimated from video recordings, such as Video S1, assuming a smooth sidewall. The scallops on the sidewalls were too small (~ 500 nm apart) to appear in the optical images (e.g., Fig. 2(a)) used for the measurement. If diffusion rate $dV(t) / dt$ can decrease to zero during the pinned stage (Stage I), the meniscus will reach a stable state and the air loss will cease. However, once the meniscus depins and proceeds to the sliding stage (Stage II), the meniscus curvature and pressure p_{tr} will not change further. Defined as the maximum immersion depth beyond which the air-water meniscus has no stable state, the critical immersion depth H_c is the depth where air diffusion rate decreases to zero at the end of Stage I. By substituting $dV(t) / dt = 0$ and $R = R_c = w / 2\cos\theta_{adv}$ into Eq. (2), we obtain:

$$H_c = \frac{2\sigma\cos\theta_{adv}}{w\rho g} + \frac{k_H c - P_{atm}}{\rho g} \tag{3}$$

where ρ is the density of water and g is the gravitational acceleration. Note that $k_H c - p_{atm}$ is the difference between the pressures of the dissolved air at the immersion depth and the

4

atmospheric air just above the water. If the dissolved air is in full equilibrium with the atmosphere so that $k_H c - p_{atm} = 0$, Eq. (3) reduces to the well-known relation below [31]:

$$H_c = \frac{2\sigma \cos\theta_{adv}}{w\rho g} \tag{4}$$

Assuming equilibrium, Eq. (4) simply states that the critical immersion depth is when the hydrostatic pressure at the depth equals the Laplace pressure sustainable by the interface at the trench. In contrast, Eq. (3) further specifies how the critical immersion depth is affected when the condition diverges from the equilibrium. Because the environmental parameters (e.g., temperature, atmospheric pressure) keep changing in reality, the dissolved air at the immersion depth is always in the process of equilibrating through diffusion, so $k_H c - p_{atm} \neq 0$ in reality. The above analysis is based on a single component gas but still applies to multiple component gases (e.g., air), because partial volumes and partial pressures can be added up in Eq. (1).
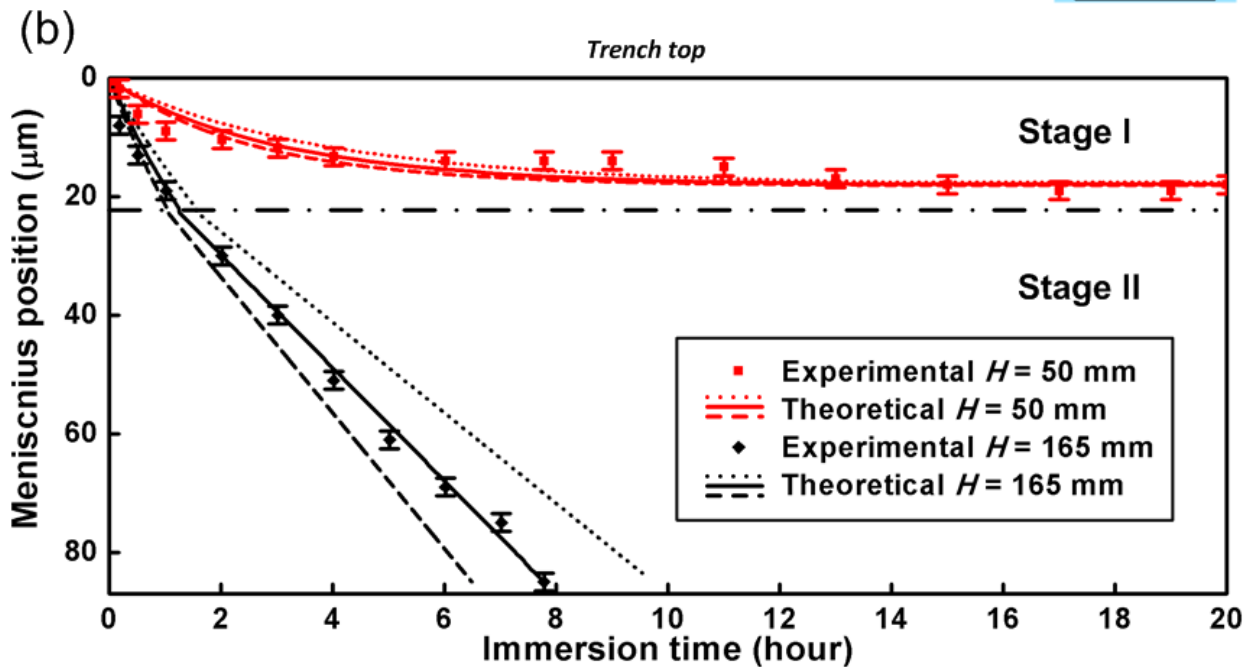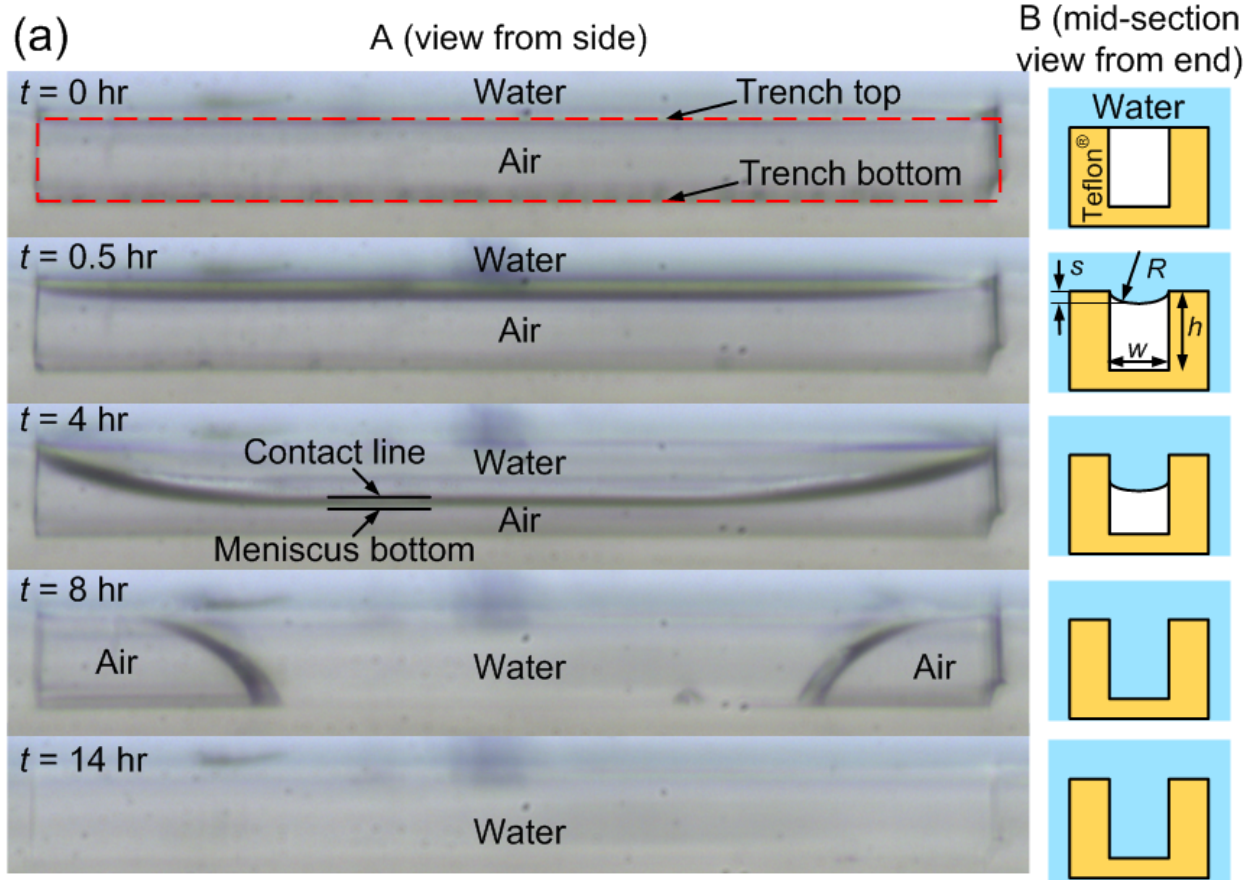
FIG. 2. Observed air depletion and trench wetting. (a) Air-water meniscus visualized by the setup shown in Fig. 1(b) with the viewing direction A shown in Fig. 1(a). Images from top to bottom show the meniscus starting to bend, depinning, sliding down, touching the trench bottom

and fully wetting the trench. Shown on the right are the corresponding cross-sectional schematics with viewing direction B. For a complete movie, see Video S1. (b) Experimental and theoretical data of the meniscus position over time reveal two distinctive stability conditions, determined by the immersion depth H. The meniscus position is defined as the distance from the top edge of the trench to the lowest position of meniscus. Experimental data were obtained from continuous microscopy images of the air-water meniscus, as shown in Fig. 2(a), using samples with $w = 147$ µm, $h = 85$ µm, and $l = 1$ mm. Uncertainty of the position measurement (~ 3 µm) is shown in the figure. Calculated for the same trench geometry and immersion depth, the solid line fit the data best with $k_p = 2.5 \times 10^{-12}$ cm/(sec•Pa), while the dotted lines show the influence of k_p with 2×10^{-12} m/(sec•Pa) and 3×10^{-12} m/(sec•Pa), respectively. The dot-dash line denotes the maximum deflection of the meniscus while the meniscus remained pinned at the top edge.

In order to elucidate the dynamic process of air depletion and trench wetting, a setup was developed to directly visualize the meniscus, as schematically illustrated in Fig. 1(b). Unlike the confocal microscopy based [7,15,29] studies, a cool LED (NuGreen Flexible Neck LED Desk Lamp, Newer Technology) was used as the light source to allow long-term observation without heating. As shown in Fig. 2(a), curved across the width of the trench, the meniscus appears as a dark strip, whose upper border is the two contact lines on the two sidewalls and whose lower border is the lowest position between the two sidewalls. When the sample was just immersed in water, the meniscus was almost flat and pinned at the top edges of the trench, as shown in the image at $t = 0$ hr. At $t = 0.5$ hr, the meniscus bent down as some of the trapped air diffused out, but the meniscus was still pinned to the top edges. As more air diffused out, the meniscus continued to bend down until finally depinning from the top edges and moving down the sidewall, as shown in the image at $t = 4$ hr. When the meniscus touched the bottom of the trench, the meniscus split into two and spread rapidly towards the ends to satisfy the local contact angle (~120°) on the bottom surface, turning the contact line along the trench length convex and in compensation making the contact line along the trench width concave. The spreading slowed down as the spreading menisci started to compress the air trapped at the corners, as suggested by the curvature change of the contact line. The trapped air continued to diffuse into the water and disappeared eventually, as shown in Video S1 in SM. In this study, we define the "lifetime" of the trapped air in the trench as the time between the moment of immersion and the moment of the meniscus touching the trench bottom. However, this definition should not be considered universal. For SHPo drag reduction, as an example, the time to the meniscus depinning, after which the designed reduction is compromised, may define the lifetime better.

In Fig. 2(b), the meniscus movement shown in Fig. 2(a) was quantified for a sample immersed at two different depths. For small immersion depth (i.e., $H = 50$ mm), the meniscus bent down and stayed relatively stable, remaining in Stage I for many hours. However, for large immersion depth (i.e., $H = 165$ mm), the meniscus bent down, depinned, moved down, and touched the bottom. The meniscus position decreased faster at the beginning during Stage I but slowed down to a constant speed (i.e., linear trend) during Stage II. The lines are drawn from Eq. (2) with $k_H c - P_{atm} = 0$, which are consistent with [27], using R_0 and k_p derived and using θ_{adv} measured in SM. In addition to helping us define the lifetime, the results in Fig. 2 confirm the theoretical model based on two stages of wetting and suggest the existence of stable menisci, i.e., infinite lifetime.

If only lifetime data of the air pocket are needed without the depletion dynamics above, the setup can be simplified by placing the sample sideways and observing the trench from above its opening with a low magnification camera, as schematically illustrated in Fig. S2 in SM. Three exemplary images captured from a video clip are shown in Fig. 3(a). The total reflection of the light from behind the sample made the meniscus in the trench appear darker to the camera, compared with the rest of the sample. These observations were confirmed consistent with the detailed dynamics of Fig. 2, validating the simplified setup, which allowed us to monitor multiples samples simultaneously and continuously in a controlled environment, as detailed in SM.
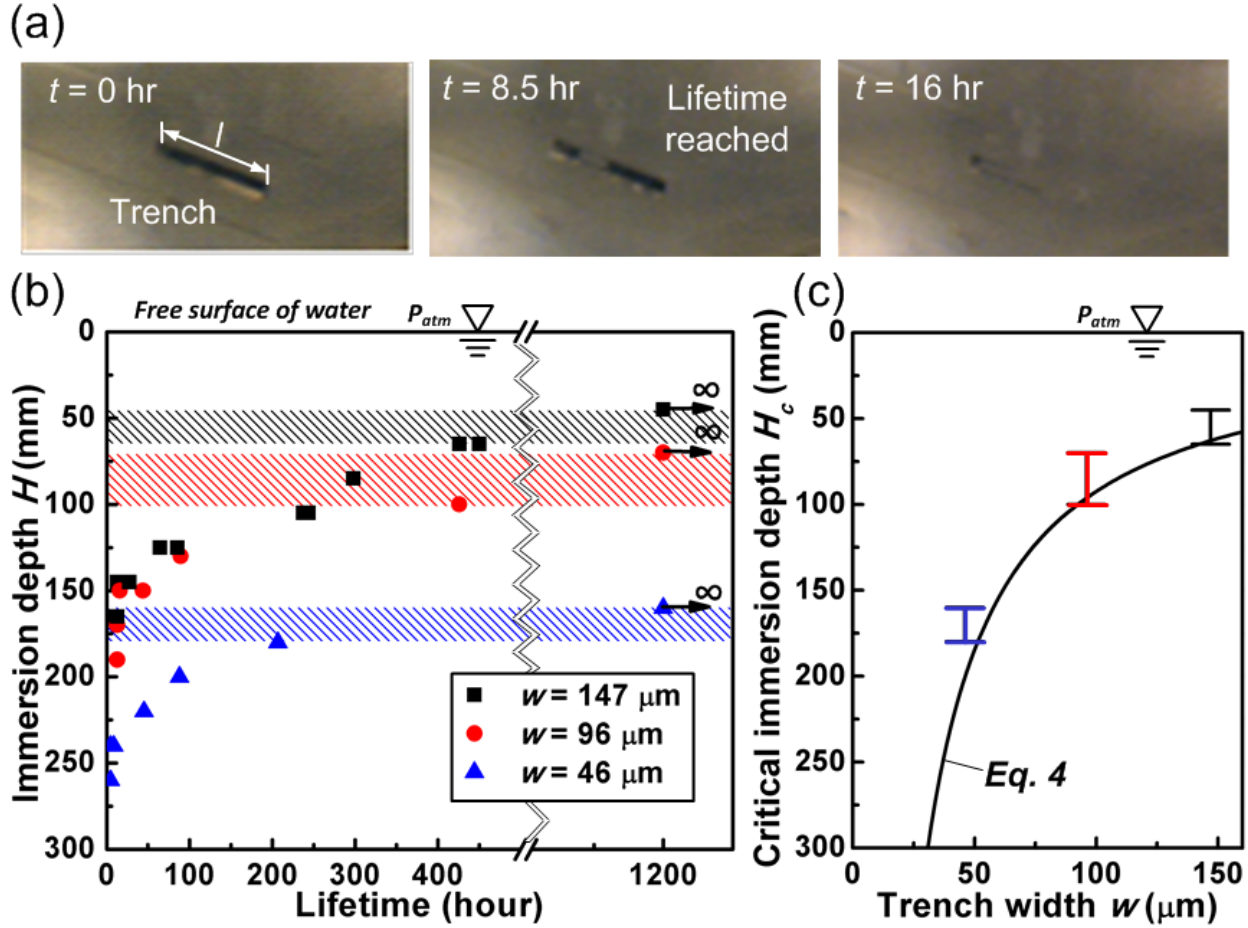
FIG. 3. Observed lifetime of trapped air. (a) Air-water meniscus seen from above the sample with low-magnification camera. The meniscus appears black. The black strip at $t = 0$ hr, the broken strip at $t = 8.5$ hr, and the disappearance of the strip at $t = 16$ hr indicate the beginning, touching bottom, and full wetting, respectively, corroborating the observation in Fig. 2(a). (b) Lifetime of trapped air as a function of immersion depth with trench width of 147 μm (■), 96 μm (●), and 46 μm (▲) as the parameter. The measurement errors of immersion depth (i.e., ± 2.5 mm due to evaporation, as explained in SM) and lifetime (i.e., the interval between snapshots) are too small to appear in the given scales. The symbols with an arrow indicate at least 1200 hours, considered infinite in this study. Each of the three colored shades indicates the uncertainty range of critical depth H_c for a given trench width. (c) Critical immersion depth H_c as a function of trench width w. The experimental results are from the uncertainty ranges (i.e., the colored shades) in (b). The solid line is the theoretical prediction of Eq. (4) with 130° as the advancing contact angle measured on the trench sidewall (obtained in SM).

Figure 3(b) shows the lifetime of the trapped air of multiple samples tested at varying immersion depths. All samples (10 mm x 5 mm x 0.5 mm Teflon® FEP piece) have one trench with the same length ($l = 1$ mm) and depth ($h \sim 85$ μm) but three different widths. For all three trench widths the lifetime increased as the immersion depth decreased, which is consistent with Eq. (3)

9

and previous experimental results [7,13,15]. However, when the immersion depth was smaller than a certain value, the trench retained the air pocket for a very long time. We declared the lifetime "infinite" after 1200 hours (50 days) and terminated the recording, but some tests were left to continue with no sign of wetting. For each trench width, the critical immersion depth H_c should be between the last data (i.e., the smallest depth) among those that became wet and the first data (i.e., largest depth) that showed an indefinite lifetime, indicating the uncertainty of measuring instability data. As shown in Fig. 3(c), the experimentally obtained ranges of H_c matched the theoretical reciprocal curve based on Eq. (4). As expected, trenches with a smaller width can be submerged deeper without losing the air pocket. Since the environmental fluctuation cannot be completely eliminated, the experimental data are slightly smaller (i.e., shallower) than the theoretically predicted depth in Fig. 3(c).

To the best of our knowledge, this is the first experimental verification of infinite lifetime of entrapped gas on microstructured surfaces fully submerged in water. Compared with previous tests, we note several aspects critical to our success. (1) The surface should be tested at a smaller depth than the critical immersion depth. However, this basic requirement was not always met before (e.g., [15]). (2) The samples in this Letter had a simple and distinctive geometry and were carefully examined to avoid any defect. Assuming a similar dimensional scale, an ordered structure is favored over random structures [7,13,14], because the latter get wetted more easily as discussed in SM. (3) Made entirely of Teflon FEP, the samples in this Letter did not need any hydrophobic coating, which is a typical source of defects for SHPo surfaces. Many used self-assembled monolayer (SAM) [14,15,31], which was found to degrade under water over time [32]. (4) The experimental procedure was carefully controlled and environmental fluctuations minimized, as detailed in SM. This extreme care was especially important when the testing depth was close to the theoretical limit.

In summary, we applied a theoretical model to describe the depletion dynamics and re-arranged it to prescribe the stable state of the air trapped in a simple hydrophobic trench under water. Then we verified the model through direct observation of air-water meniscus and experimentally obtained a stable air pocket in the trench. The lifetime of the air pocket was obtained as function of immersion depth with the trench width as a parameter. The infinite lifetime (> 1200 hours)

was obtained by minimizing the environmental fluctuations in the experiments. The critical immersion depth, within which the indefinite plastron is possible, was confirmed to depend reciprocally on the trench width. While verifying that the indefinite plastron can exist as predicted by the theoretical model, this study conversely attests to the delicate fragility of the plastron on SHPo surfaces. To keep a plastron stable under realistic conditions, where environmental parameters would fluctuate significantly, one should use the SHPo surface at a much shallower depth than the theoretical critical immersion depth. Although performed under a near thermodynamic equilibrium environment far from realistic conditions, this study nevertheless teaches us (1) that the indefinite SHPo state does exist, (2) how to design SHPo surfaces to retain the air better, and (3) that the indefinite SHPo state would not be possible for many applications unless energetically assisted [16]. In particular for drag reduction, which requires a trench width larger than ~20 μm [18], the results indicate long-term (e.g., > days) operations are not possible in field conditions unless the immersion is very shallow (e.g., mere centimeters) or the gas is replenished [16].

*Correspondence to: cjkim@ucla.edu

[1]   We abbreviate superhydrophobic to SHPo in order to differentiate it from superhydrophilic (SHPi) as well as the likes of superlyophobic and superoleophobic.
[2]   L. Bocquet and E. Lauga, Nature Materials **10**, 334 (2011).
[3]   C. Lee, C.-H. Choi, and C.-J. Kim, Phys Rev Lett **101**, 64501 (2008).
[4]   R. J. Daniello, N. E. Waterhouse, and J. P. Rothstein, Physics of Fluids **21**, 085103 (2009).
[5]   E. Karatay, A. S. Haase, C. W. Visser, C. Sun, D. Lohse, P. A. Tsai, and R. G. H. Lammertink, P Natl Acad Sci USA **110**, 8422 (2013).
[6]   K. Koch and W. Barthlott, Philos T R Soc A **367**, 1487 (2009).
[7]   R. Poetes, K. Holtzmann, K. Franze, and U. Steiner, Phys Rev Lett **105**, 166104 (2010).
[8]   Y. H. Xue, S. G. Chu, P. Y. Lv, and H. L. Duan, Langmuir **28**, 9440 (2012).
[9]   W.-Y. Sun and C.-J. Kim, in *Proc. IEEE Conf. MEMS* (IEEE, Taipei, Taiwan, 2013), pp. 397.
[10]   M. A. Samaha, H. V. Tafreshi, and M. Gad-el-Hak, Langmuir **28**, 9759 (2012).
[11]   F. O. Ochanda, M. A. Samaha, H. V. Tafreshi, G. C. Tepper, and M. Gad-el-Hak, Journal of Applied Polymer Science **124**, 5021 (2012).

[12]   A. Balmert, H. Florian Bohn, P. Ditsche-Kuru, and W. Barthlott, Journal of Morphology **272**, 442 (2011).

[13]   M. A. Samaha, H. V. Tafreshi, and M. Gad-el-Hak, Physics of Fluids **24**, 112103 (2012).

[14]   M. S. Bobji, S. V. Kumar, A. Asthana, and R. N. Govardhan, Langmuir **25**, 12120 (2009).

[15]   P. Lv, Y. Xue, Y. Shi, H. Lin, and H. Duan, Phys Rev Lett **112**, 196101 (2014).

[16]   C. Lee and C.-J. Kim, Phys Rev Lett **106**, 14502 (2011).

[17]   B. Woolford, J. Prince, D. Maynes, and B. W. Webb, Physics of Fluids **21**, 085106 (2009).

[18]   H. Park, G. Sun, and C.-J. Kim, Journal of Fluid Mechanics **747**, 722 (2014).

[19]   E. Aljallis, M. A. Sarshar, R. Datla, V. Sikka, A. Jones, and C. H. Choi, Physics of Fluids **25**, 025103 (2013).

[20]   C.-H. Choi and C.-J. Kim, Phys Rev Lett **96**, 066001 (2006).

[21]   F. Scholz, *Electroanalytical methods: guide to experiments and applications* (Springer, 2009).

[22]   R. D. Deegan, O. Bakajin, T. F. Dupont, G. Huber, S. R. Nagel, and T. A. Witten, Nature **389**, 827 (1997).

[23]   K. N. Ren, W. Dai, J. H. Zhou, J. Su, and H. K. Wu, P Natl Acad Sci USA **108**, 8162 (2011).

[24]   W. Feast, H. Munro, and R. W. Richards, *Polymer surfaces and interfaces II* (Wiley, 1993), Vol. 2.

[25]   M. J. Madou, *Fundamentals of microfabrication: the science of miniaturization* (CRC press, 2002).

[26]   M. Flynn and J. W. Bush, Journal of Fluid Mechanics **608**, 275 (2008).

[27]   B. Emami, A. Hemeda, M. Amrei, A. Luzar, M. Gad-el-Hak, and H. V. Tafreshi, Physics of Fluids **25**, 062108 (2013).

[28]   R. Picknett and R. Bexon, Journal of Colloid and Interface Science **61**, 336 (1977).

[29]   P. Papadopoulos, L. Mammen, X. Deng, D. Vollmer, and H.-J. Butt, Proceedings of the National Academy of Sciences **110**, 3254 (2013).

[30]   M. Reyssat, J. M. Yeomans, and D. Quere, Europhys. Lett. **81**, 26606 (2008).

[31]   H. Rathgen and F. Mugele, Faraday Discuss **146**, 49 (2010).

[32]   B. Kobrin, J. Chin, and W. Ashurst, in *World Tribology Congress III* (American Society of Mechanical Engineers, Washington, D.C., USA, 2005), pp. 533.

[33]   See Supplemental Material [url], which includes Refs. [34-36].

[34]   E. L. Cussler, *Diffusion: mass transfer in fluid systems* (Cambridge university press, 2009).

[35]   P. B. Duncan and D. Needham, Langmuir **20**, 2567 (2004).

[36]   T. Enns, P. F. Scholander, and E. D. Bradstreet, The Journal of Physical Chemistry **69**, 389 (1965).

Supplemental Materials for

Infinite Lifetime of Underwater Superhydrophobic State

Muchen Xu, Guangyi Sun, and Chang-Jin "CJ" Kim [*]

Mechanical and Aerospace Engineering Department
University of California at Los Angeles, (UCLA), Los Angeles, CA 90095, USA
*Correspondence to: cjkim@ucla.edu

Contents:

MATERIALS AND METHODS

Fabrication of Teflon® FEP single-trench sample

The single-trench sample was fabricated from Teflon® FEP by hot embossing with a silicon mold, as illustrated in Fig. S1. The mold was fabricated by deep reactive ion etching (DRIE) on a 500 µm-thick silicon wafer using photoresist as etching mask. A thin Teflon® FEP sheet (McMaster-Carr Supply Co., Inc.) was pressed into the silicon mold at temperature higher than its glass transition temperature (265 ℃ [S1]). After transferring the silicon-FEP-glass onto a cold plate and allowing a cooldown, the Teflon® FEP sample was manually demolded from the silicon mold. The resulting sample is semi-transparent and intrinsically hydrophobic with advancing contact angle on smooth surface ~ 115° [S2].
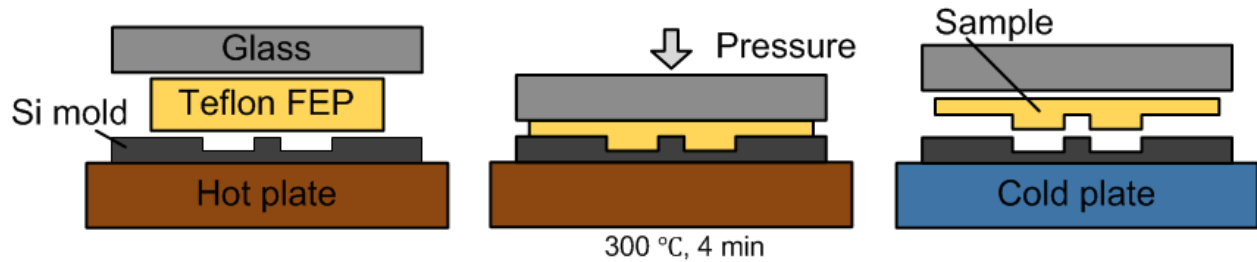
FIG. S1. Molding process to form an optically clear Teflon® FEP single-trench sample. Silicon mold is ~500 μm thick; glass plate is ~1 mm thick; and Teflon® FEP sample is around 10 mm x 5 mm x 0.5 mm.

Simplified visualization setup to monitor the lifetime of air pocket

In order to obtain the lifetime data under uniform conditions efficiently, all the samples were tested simultaneously in 19 tubes of varying water levels, using multiple low-cost cameras (Dino-Lite®) as shown in Fig. S2. Two identical samples, i.e., of an identical trench geometry, were placed in a tube to produce two data points for each of all test conditions. Although this setup does not provide the vertical position or shape information of the meniscus shown in Fig. 2, it can still conclusively determine whether the meniscus touched the bottom of the trench, i.e., reached the lifetime, as confirmed in the detailed study of the meniscus described in the main text. Since the samples were placed vertically in the tube for the lifetime tests for convenience (e.g., to fit in the narrow bottom of the tube, make the sample handling easier, and ease the adjustment of lighting, etc.), the immersion depth varied along the channel length. However, the channel length ($l = 1$ mm) was much smaller than the immersion depth ($H > 50$ mm) so that the length effect was negligible in the lifetime data.

Minimizing environmental fluctuation

The meniscus stability in the trench was found to be very sensitive to environment fluctuations, especially if the surrounding water was of a large amount. When various parameters (e.g., pressure, temperature) of the environment change, the corresponding parameters in the water (e.g., the dissolved gas concentration, temperature) change slowly with a time lag. The lagging responses make the states of water at a given moment somewhat different from the states of water in full equilibrium with the surrounding, leading to a deviation from the theoretical model,

which was based on full equilibrium. In order to emulate the equilibrium states as close as possible, the experiment was carried out with small-diameter (~1.5 cm) tubes in an enclosed lab bench with no air flow, no agitations, and minimal temperature variations. Deionized water was left in the bench for a minimum of 2 days before using so that the water is fully saturated with surrounding air [S3]. The temperature (21.3 ± 0.5 ℃) and relative humidity (53 ± 3 %) in the lab bench were monitored throughout the experiment (> 1200 hours) using a barometer (Wireless Weather Forecaster, SpringField Precision, Inc.). In order to compensate for the water loss by evaporation, which decreases the immersion depth, the tubes were refilled once a day using a water bottle kept in the same bench with the tubes. The variation of the water level in the tube was less than ~ 5 mm throughout the experiment.
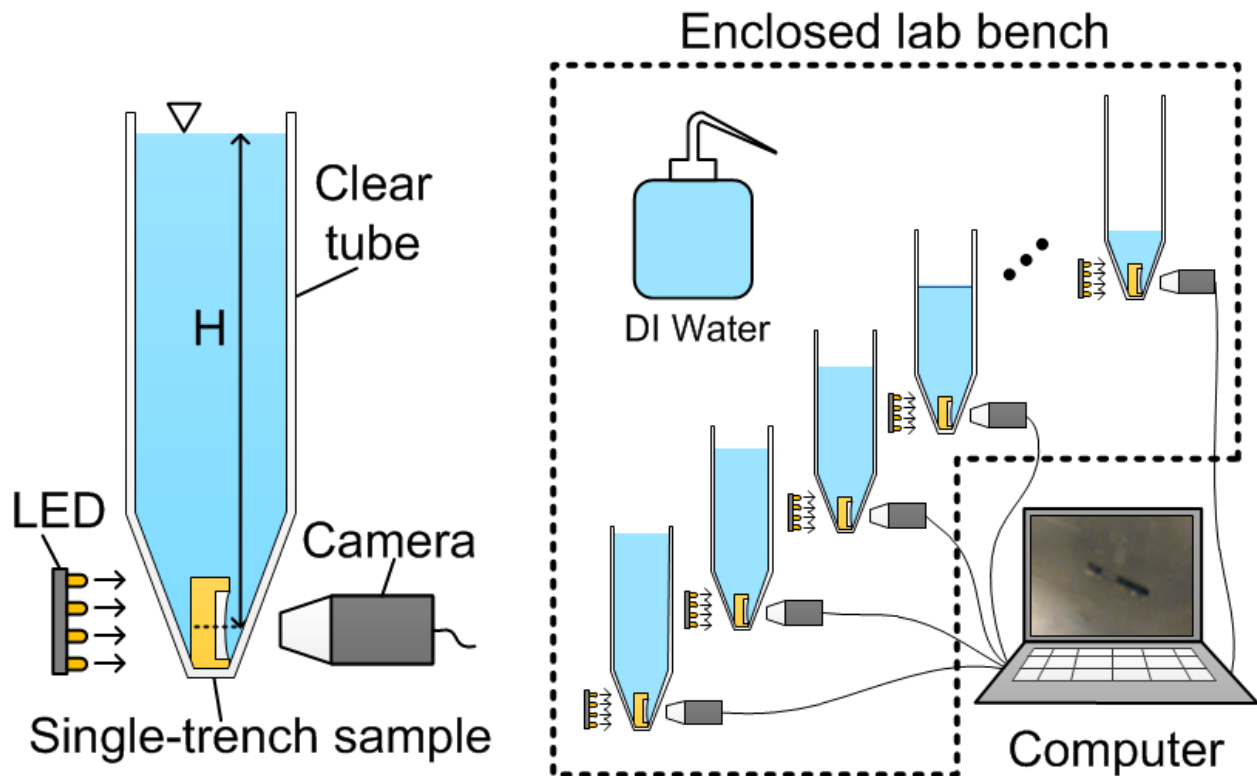

FIG. S2. Schematic illustration of the experimental setup to monitor the lifetime. Each tube has two identical samples (although only one is drawn for clarity) at the bottom and is filled with water to an assigned height H. By employing multiple cameras, 38 samples were monitored simultaneously for the entire testing period (> 1200 hours). Water loss by evaporation was compensated once a day using the reserve water in a bottle kept in the same bench throughout the experiment.

THEORY OF AIR DEPLETION IN TRENCH

Initial curvature of the air-water interface

When the above-prepared Teflon FEP sample is immersed in water, the air at atmospheric pressure is entrapped in the microscopic trench. Assuming the sample surface crosses the free surface of water very slowly so that the trench is closed off with a flat air-water meniscus, we can say at the crossing the trapped air has the pressure of atmosphere p_{atm} and the volume of trench V_{tr} determined by the trench width w, depth h, and length l. As the sample is lowered to depth H, the trapped air is compressed by the hydrostatic pressure p_H to a volume of V_0 at $p_{tr,0}$ at time $t = 0$. If the meniscus is pinned at the top edge of the trench, the compression makes the meniscus bend down into the trench, and the capillary pressure by the air-water interfacial tension σ helps counter the hydrostatic pressure. Assuming the air is ideal gas and compressed isothermally [S4], Laplace equation and the ideal gas law lead to:

$$p_{atm} + p_H - p_{tr,0} = \sigma / R_0 \tag{S1}$$

$$p_{atm}V_{tr} = p_{tr,0}V_0 \tag{S2}$$

By combining Eqs. (S1) and (S2), the initial radius of curvature R_0 after submerging the sample to a depth H can be calculated as:

$$R_0 = \frac{s}{p_{atm}(1 - V_{tr}/V_0) + p_H} \tag{S3}$$

where V_0 can be expressed in terms of V_{tr} and R_0. Since $V_0 \leq V_{tr}$ and $R_0 \geq \sigma / p_H$ with the equality for an infinitely deep trench (i.e., $h \rightarrow \infty$), this equation indicates that at fresh immersion (i.e., before diffusion starts) the meniscus bends down less on a shallow trench than on a deep trench.

Calculation of the meniscus area and position

Based on the 2D schematics in the right column named "B (midsection view from end)" of Fig. 2(a), i.e., assuming an infinitely long trench, the area of the meniscus A and the volume of the trapped air V can be obtained from the trench dimensions and the radius of curvature of the meniscus R as:

$$A = 2R \arcsin(\frac{w}{2R}) \tag{S4}$$

$$V = wh - [R^2 \arcsin(\frac{w}{2R}) - \frac{w}{2}\sqrt{R^2 - \frac{w^2}{4}}] \tag{S5}$$

The rate of the air volume change can be expressed as the rate of the meniscus radius change as:

$$\frac{dV(t)}{dt} = \frac{dV(R)}{dR} \cdot \frac{dR(t)}{dt} \tag{S6}$$

where $dV(R)/dR$ can be obtained from Eq. (S5). After substituting Eq. (S6) into Eq. (2), the resulting first-order differential equation was solved numerically for R, and the meniscus position s was calculated from

$$s = R - \sqrt{R^2 - (w/2)^2} \tag{S7}$$

and drawn in Fig. 2(b) as theoretical curves.

Interface diffusion coefficient

The interface diffusion coefficient k_p is affected by the meniscus curvature, as studied in the diffusion-limited drop evaporation theory [S5], which assumed quasi-stationary, diffusion-controlled evaporation in still air. Its boundary conditions at the meniscus and infinity were similar to our study. In the theory, the mass transfer rate is:

$$\frac{dm(t)}{dt} = -\frac{kr_0(C/r)\sin\theta_0}{2\sin\theta} \tag{S8}$$

where θ is the angle of meniscus with respect to the horizontal surface with θ_0 as its initial value, r is the meniscus radius with r_0 as its initial value, and k is a constant. Related to θ, C/r has its empirical polynomial estimated from [S5]. The ratio between two mass transfer rates of two different curvatures is:

$$K = (\frac{dm}{dt})_1 / (\frac{dm}{dt})_2 = \frac{C_1/(r_1\sin\theta_1)}{C_2/(r_2\sin\theta_2)} \tag{S9}$$

When the meniscus is flat so that θ_1 is 0°, $C_1 / (r_1 \sin\theta_1) = 2/\pi \simeq 0.63$ [S5]. When the meniscus forms the advancing contact angle on the trench sidewall (θ_{adv} = 130° in this study) so that θ_2 is 40°, $C_2 / (r_2 \sin\theta_2) \simeq 0.73$, and the ratio K is about 0.86. However, this result is for a spherical droplet. Having about half the value, the curvature of the meniscus on the long trench of this Letter is expected to affect the mass diffusion rate less than the above discussion. To calculate the interface diffusion coefficient k_p, we eventually used the diffusion length, which assumes a constant mass transfer rate and was used in recent work [S6]. The interface diffusion coefficient k_p can be estimated using "film theory" for mass transfer across interfaces [S7]:

$$k_p = \frac{D}{\delta} \cdot \frac{M}{k_H \rho_{air}} \tag{S10}$$

Here, δ is the "diffusion length", typically around 0.1 mm for short diffusion time (i.e., ~ 10^3 s) [S6,7]. Other values are obtained from reference [S8] measured at 22 °C: M is the molecular weight of air (i.e., 29 g/mol); ρ_{air} is the density of air (i.e., 0.0012 g/cm^3); D is the diffusion constant of air in water (i.e., 1.75–2.00×10^{-5} cm^2/s); and k_H is Henry`s constant (i.e., 1.21–1.34 atm/mM). Henry`s constant is invariant of hydrostatic pressure, unless the immersion depth is very large (e.g., H_r only increases by 14% at ~1000 m of water depth [S9]). By substituting these values in Eq. (4), k_p is calculated to be around 3×10^{-12} m/(sec•Pa), which is around the extracted value from Fig. 2(b) or 2.5×10^{-12} m/(sec•Pa).

Advancing contact angle on sidewall

The advancing contact angle θ_{adv} on the trench sidewall was determined by observing an air bubble shrinking inside the trench. Figure S3 shows an image right before the bubble depinned from the top edge of the trench. The advancing contact angle was measured to be ~130°, larger than that on a smooth Teflon® FEP surface (~115° [S2]) because of the rough sidewall shown in Fig. 1(a).
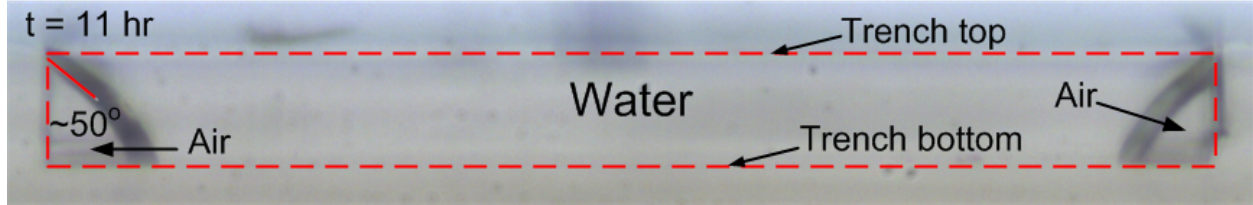
FIG. S3. Measurement of advancing contact angle on trench sidewall. The advancing contact angle was read using the bubbles shrinking at the two ends of the trench after the meniscus touched the bottom. The picture is the frame when the left bubble's triple contact line at the top edge of the trench was about to depin. The advancing contact angle is estimated to be ~130°. The right bubble had already depinned.

Surface topography and plastron robustness

It would be informative to relate the current results with different surfaces reported in the literature, e.g., schematically drawn for random protrusions of lotus-leaves-like surfaces [S10] in Fig. S4(a) and parallel microtrichia of underwater insect skins [S11,12] in Fig. S4(c). Assuming same material (i.e., same contact angle) and similar structure spacing, their morphologies would determine the critical radii of curvature R_c and thus the critical immersion depth H_c. For the random structures of Fig. S4(a), the sloped sidewalls and non-uniform heights make R_c larger and H_c smaller. On the other hand, for the parallel structures of Fig. S4(c), the re-entrance of the structures makes R_c smaller and H_c larger, explaining the observation for indefinite plastron. Importantly, the habitat of these underwater insects is much shallower (e.g., $H \sim 15$ cm [S11]) than the H_c value calculated from their surface structures (e.g., $H_c > 15$ m for ~0.5 μm microtrichia [S11], assuming local advancing contact angle of 120°). We speculate that the large safety factor (~100×) helps their plastron resist the large environmental fluctuations present in nature.
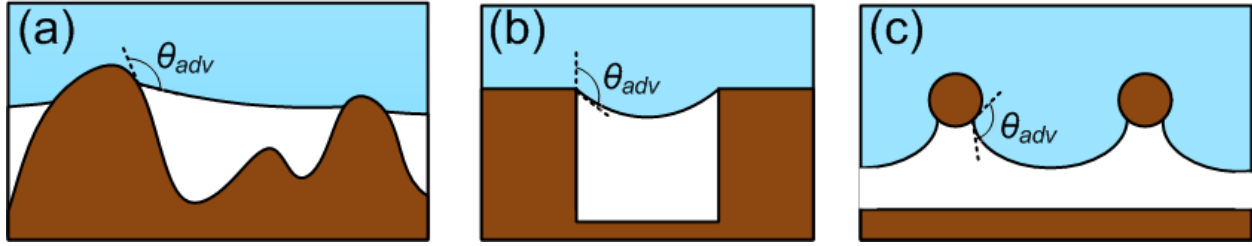
FIG. S4. Schematic representations of three different SHPo surfaces of same material with different surface topography and corresponding air-water meniscus shape. (a) SHPo surface with random protrusions (e.g., [S10]) with slightly convex meniscus can hardly support any hydrostatic pressure unless the spacing is in nanometer scale. (b) Trench structure with reasonable convex meniscus (e.g., this study) can support some hydrostatic pressures with spacing in micrometer scale. (c) Parallel setae with highly convex meniscus (e.g., [S11,12]) and micrometer scale spacing can support more hydrostatic pressure due to their re-entrant shape. In reality, the environmental fluctuations make the air depleted much easier than the theory based on the equilibrium state. As result, the indefinite retention of the air was observed only when the environmental fluctuation was minimized for (b) (this study) or when the spacing was in nanometer scale for (c) [S11,12].

References

[S1] K. N. Ren, W. Dai, J. H. Zhou, J. Su, and H. K. Wu, *P Natl Acad Sci* USA **108**, 8162 (2011).

[S2] W. Feast, H. Munro, and R. W. Richards, *Polymer surfaces and interfaces II* (Wiley, 1993), Vol. 2.

[S3] M. S. Bobji, S. V. Kumar, A. Asthana, and R. N. Govardhan, *Langmuir* **25**, 12120 (2009).

[S4] B. Emami, A. Hemeda, M. Amrei, A. Luzar, M. Gad-el-Hak, and H. V. Tafreshi, *Physics of Fluids* **25**, 062108 (2013).

[S5] R. Picknett and R. Bexon, Jour*nal of Colloid and Interface Science* **61**, 336 (1977).

[S6] P. Lv, Y. Xue, Y. Shi, H. Lin, and H. Duan, *Phys Rev Lett* **112**, 196101 (2014).

[S7] E. L. Cussler, *Diffusion: mass transfer in fluid systems* (Cambridge Univ. Press, 2009).

[S8] P. B. Duncan and D. Needham, *Langmuir* **20**, 2567 (2004).

[S9] T. Enns, P. F. Scholander, and E. D. Bradstreet, *The Journal of Physical Chemistry* **69**, 389 (1965).

[S10] R. Poetes, K. Holtzmann, K. Franze, and U. Steiner, *Phys Rev Lett* **105**, 166104 (2010).

[S11] A. Balmert, H. Florian Bohn, P. Ditsche-Kuru, and W. Barthlott, *Journal of Morphology* **272**, 442 (2011).

[S12] M. Flynn and J. W. Bush, *Journal of Fluid Mechanics* **608**, 275 (2008).